



Efficient scale-up synthesis and hydrogen separation of hollow fiber DD3R zeolite membranes



Peng Du^a, Jieyu Song^a, Xuerui Wang^a, Yuting Zhang^a, Jixian Xie^a, Gang Liu^b, Yongli Liu^b, Zhenwei Wang^b, Zhou Hong^c, Xuehong Gu^{a,*}

^a State Key Laboratory of Materials-Oriented Chemical Engineering, College of Chemical Engineering, Nanjing Tech University, Nanjing, 211816, Jiangsu, China

^b Sinopec Engineering Incorporation, Beijing, 100101, China

^c Nanjing Membrane Materials Industrial Technology Research Institute Co., Ltd., Nanjing, 211800, Jiangsu, China

ARTICLE INFO

Keywords:

Zeolite membrane
DDR zeolite
Hollow fiber
Hydrogen
Gas separation

ABSTRACT

Efficient hydrogen (H_2) separation is highly desired from the cracked tail gas of ethylene plant. In this work, DD3R zeolite membranes have been evaluated for potential application in H_2 separation under harsh conditions. We developed an efficient scale-up synthesis of hollow fiber DD3R zeolite membranes. The alkalinity of synthesis solution was optimized to endow the good reproducibility of high-quality membranes. 17 pieces of separate membranes, total 406 cm^2 , were synthesized in one autoclave using the industrial grade agents. Typically, the 25 cm long membrane showed CO_2/CH_4 selectivity of 447 and CO_2 permeance of $1.55 \times 10^{-7}\text{ mol m}^{-2}\text{ s}^{-1}\text{ Pa}^{-1}$. The single component permeance of H_2 is $1.8 \times 10^{-8}\text{ mol m}^{-2}\text{ s}^{-1}\text{ Pa}^{-1}$ at 303 K and feed pressure of 0.4 MPa, leading to the ideal selectivity of 124 for H_2/CH_4 , 242 for H_2/C_2H_4 and 424 for H_2/C_2H_6 . For the simulated cracked gas, H_2 permeance and H_2/CH_4 separation selectivity was $1.25 \times 10^{-8}\text{ mol m}^{-2}\text{ s}^{-1}\text{ Pa}^{-1}$ and 128, respectively. More importantly, the DD3R zeolite membrane was stable for more than 1000 h in the simulated cracked gas containing 100 ppm H_2S . Together with the linear increase of H_2 flux and H_2/CH_4 separation selectivity of 50 at high pressure of 2.1 MPa, DD3R zeolite membranes pave the way to H_2 separation from ethylene industry.

1. Introduction

Hydrogen (H_2) separation is an important step in the process of ethylene production. The feedstock of naphtha is thermally cracked to generate light hydrocarbons and H_2 . High-purity ethylene is obtained after the impurity removal by cryogenic distillation. However, the process is energy extensive because of the low temperature of 108 K required. From the perspective of energy saving, it is highly desired to separate H_2 from the light hydrocarbons before the subsequent cryogenic distillative purification of hydrocarbons [1].

Physical adsorption is deemed an energy-efficient alternative that can be operated at near-ambient conditions [2]. However, the H_2 content in the cracked gas is approximate 20%, which is only 25% of the strong-adsorption hydrocarbons, including CH_4 , C_2H_4 , C_2H_6 . In this case, the adsorption column will break through in a short period and need to be regenerated frequently. Alternatively, membrane separation is more energy-efficient because only the fast H_2 component permeates through and no phase transition occurs [3]. The membrane separation

can achieve a better H_2 recovery of 95% compared to 79% using pressure swing adsorption [4]. Because of the low flexibility and rigid chain-packing structure, the H_2 permeability is merely 10 barrer for the commercial membranes such as poly (ethylene imine) (PEI), polyethersulfone (PES) and polybenzimidazole (PBI) [5].

Zeolite membranes featured with well-defined channels are the most promising candidate for H_2 separation in terms of working capacity (flux) and efficiency (selectivity) [6–8]. MFI zeolite membranes were competent for H_2/CO_2 separation at high temperature after the internal surface modification [9]. Yu et al. prepared microporous Al_2O_3 -SAPO-34 zeolite composite membranes for H_2/N_2 separation using molecular layer deposition [10]. Kapteijn et al. claimed the small-pore DD3R zeolite membranes offered H_2 permeance of $4.5 \times 10^{-8}\text{ mol m}^{-2}\text{ s}^{-1}\text{ Pa}^{-1}$ and the ideal H_2 /isobutane selectivity was up to 500 [11]. Because of the molecular sieving mechanism H_2 permeation was insensitive to the presence of isobutane at high temperature. While the components of C_2H_4 and C_2H_6 in the cracked gas can enter the pore of DD3R zeolite because of the smaller kinetic diameters (C_2H_4 : 0.42 nm,

* Corresponding author.

E-mail address: xhgu@njtech.edu.cn (X. Gu).

C_2H_6 : 0.44 nm), its effect on H_2 permeation through DD3R zeolite membranes was unclear yet.

DD3R zeolite membranes were firstly synthesized for CO_2/CH_4 separation in 2004 [12]. Nevertheless, the reproducible synthesis of large scale DD3R zeolite membranes is still challenging [13]. The challenges in successful synthesis of DD3R membranes mainly focus on competitive formation of impurity phase such as Sigma-2 (SGT) in the membrane and thermal-induced intercrystalline defects after air calcination at high temperature (as high as 700 °C) [14]. To address these issues, we proposed a combined synthesis strategy of hydrothermal synthesis in a dilute precursor followed by low-temperature (200 °C) detemplation in ozone/oxygen mixed atmosphere [15]. As a result, pure-phase DD3R membranes were prepared with high reproducibility. The scale-up preparation of DD3R zeolite membranes is essential to realize the H_2 separation from hydrocarbons in the ethylene plant.

Here, we reported an efficient scale-up approach of DD3R zeolite membranes for hydrogen separation from light hydrocarbons. The dilute synthesis solution as our previous report was used [15], while the alkalinity was further optimized to prepare high-quality membranes. The effective length of hollow fiber DD3R zeolite membranes were extended to 25 cm. One autoclave produced 17 separate membranes, with total area of 406 cm². The reliability of our approach was demonstrated by three independent batch-synthesis. The membrane quality was evaluated by single component permeation, binary and multi-component separation. The effects of hydrocarbons (CH_4 , C_2H_4 , C_2H_6) on H_2 permeation were investigated. More importantly, the membrane resistance to H_2S and high pressure was explored.

2. Experimental

2.1. Synthesis of DD3R zeolite membranes

In this study, two kinds of hollow fiber DD3R zeolite membranes were synthesized. The short one (the membrane length of 5 cm) was used to optimize the alkalinity of synthetic solution, while the other one (the membrane length of 25 cm) was used in the scaled-up synthesis. The four-channel α -Al₂O₃ hollow fiber supports with 3.8 mm O.D., 0.9 mm I.D., ~50% porosity and an average pore size of 200 nm were provided from *Nanjing Membrane Materials Industrial Technology Research Institute Co., Ltd*. The synthesis procedure was similar to our previous study [15, 16]. Ball-milled Sigma-1 zeolite (average particle size of 0.5 μm) was planted on the substrate outer surface by dip-coating approach with an 0.5 wt% seed suspension for 15 s. The molar composition of the synthesis solution was 100 SiO₂: 3 ADA (1-adamantanamine): 50 EDA (ethylenediamine): 4000 H₂O: x (0.95–3.03) Na₂O (sodium oxide). Industrial grade chemical was used to synthesis. The property of industrial grade colloidal silica was shown in Table 1 and it contains 0.39% Na₂O and gives a SiO₂/Na₂O ratio of 105. The alkalinity of solution was further adjusted by adding extra NaOH to the synthesis solution. After ageing, 30 mL (the membrane length of 5 cm) and 1200 mL (the membrane length of 25 cm) synthetic solution was poured in stainless steel autoclave.

The hydrothermal crystallization was carried out at 413 K for 44 h. The structural directing agents (SDAs) trapped in the zeolite pores were decomposed in ozone atmosphere at 473 K for 80 h. Ozone was produced by an electrical discharge generator (Lvbang, NPO50P-S-2), where ~140 g m⁻³ ozone was mixed with oxygen to give a flow rate of 2 L min⁻¹.

Table 1
Industrial grade silica source used in our synthesis.

| SiO ₂ /wt% | Na ₂ O/wt% | pH | Particle size/nm |
|-----------------------|-----------------------|------|------------------|
| 40 | 0.39 | 10.4 | 15 |

2.2. Gas separation performance test

The as-synthesized membrane was mounted in a stainless-steel module, with each end sealed by a silicone O-ring. The single gas permeation was tested using a transient permeation apparatus without sweep gas. The mixture gas separation was performed in a Wicke-Kallenbach gas separation apparatus. The temperature was adjusted by a furnace in the range of 298–373 K while a refrigerator was used to cool the module to 243 K. The feed pressure was modulated by a back pressure regulator, and the permeate side was operated under atmospheric pressure. For equimolar mixture separation, the total flow rate was 200 mL min⁻¹, and a helium stream (100 mL min⁻¹) was used to sweep the permeate side. All the flow refers to the volume flow under normal temperature pressure (NTP).

A gas chromatography (GC, 7820A, Agilent Technologies), equipped with thermal conductivity detector (TCD) and a packed column of HAYESEP-DB, was used to analyse gas compositions. The gas permeance of component i (P_i) is defined as:

$$P_i = \frac{J_i}{\Delta p_i} \quad (1)$$

where J_i is the flux of component i (mol m⁻² s⁻¹), and Δp_i is the transmembrane partial pressure difference for component i (Pa). The ideal selectivity ($S_{i/j}$) and mixture selectivity ($\alpha_{i/j}$) of component i over component j is defined as:

$$S_{i/j} = \frac{P_i}{P_j} \quad (2)$$

$$\alpha_{i/j} = \frac{P_i}{P_j} \quad (3)$$

where P_i and P_j are the gas permeance (mol m⁻² s⁻¹ Pa⁻¹) of component i and j, respectively.

In the case of high-pressure H_2/CH_4 mixture separation, the feed flow was controlled at 1500 mL min⁻¹. The permeate pressure was fixed at atmospheric and no sweep gas was used. The gas flow rate of permeate was measured by bubble flow meter. The permeate and retentate were analyzed by a gas chromatograph (GC, 7820A, Agilent Technologies, with HAYESEP-DB). Considering the variation of gas composition along the membrane (especially at high pressure), we used the logarithmic average to calculate Δp_i [17].

$$\Delta p_i = \frac{(p_i^{\text{feed}} - p_i^{\text{perm}}) - (p_i^{\text{ret}} - p_i^{\text{perm}})}{\ln \left(\frac{p_i^{\text{feed}} - p_i^{\text{perm}}}{p_i^{\text{ret}} - p_i^{\text{perm}}} \right)} \quad (4)$$

The relative reduction of P_i (ΔP_i) was defined as:

$$\Delta P_i = \frac{|P_i' - P_i|}{P_i} \quad (5)$$

where P_i' is the gas permeance of component i after the addition of ethane or ethylene into H_2/CH_4 binary mixture.

2.3. Membrane characterization

The morphologies of the membranes were examined via FESEM (S4800, Hitachi, Japan). The working voltage (HV) of 5 kV and distance (WD) of 8 mm were used. Elemental compositions of the zeolite membranes were analyzed by EDX (EMAX x-act, Horiba). Prior to EDX test, all the samples were washed with DI water carefully. The crystal phases were determined by X-ray diffraction (XRD, MiniFlex 600, Rigaku) with $Cu K_\alpha$ radiation in the 2θ range of 5–50°. Gas adsorption isotherms were obtained using a BELSORP volumetric adsorption instrument (BEL Japan Corp.).

3. Results and discussion

3.1. Optimization of alkalinity for DD3R zeolite membrane synthesis

The DD3R zeolite crystallinity and morphology are sensitive to the silica source [18,19]. Gascon et al. [18] claimed a strict requirement on alkalinity of the colloidal silica to prevent the impurity phase. Furthermore, it will affect the alkalinity of the synthesis solution due to the difference in Na_2O content, which is deemed as a key factor to determine

the zeolite morphology [19,20]. In this work, industrial grade colloidal silica was used to reduce the cost of preparing zeolite membranes. The $\text{SiO}_2/\text{Na}_2\text{O}$ ratio was controlled between 105 and 33. The thicknesses of the synthesized membranes were in the range of 5–6 μm (Fig. 1b, d, f and h), similar to the membranes synthesized from analytical reagent (AR) grade silica source [16]. The slight fluctuation could be attributed to the seeding quality as it is sensitive to the support roughness and porosity [21,22]. However, the surface morphology evolved from the typical triangle to irregular grains with decreasing $\text{SiO}_2/\text{Na}_2\text{O}$ ratio. The

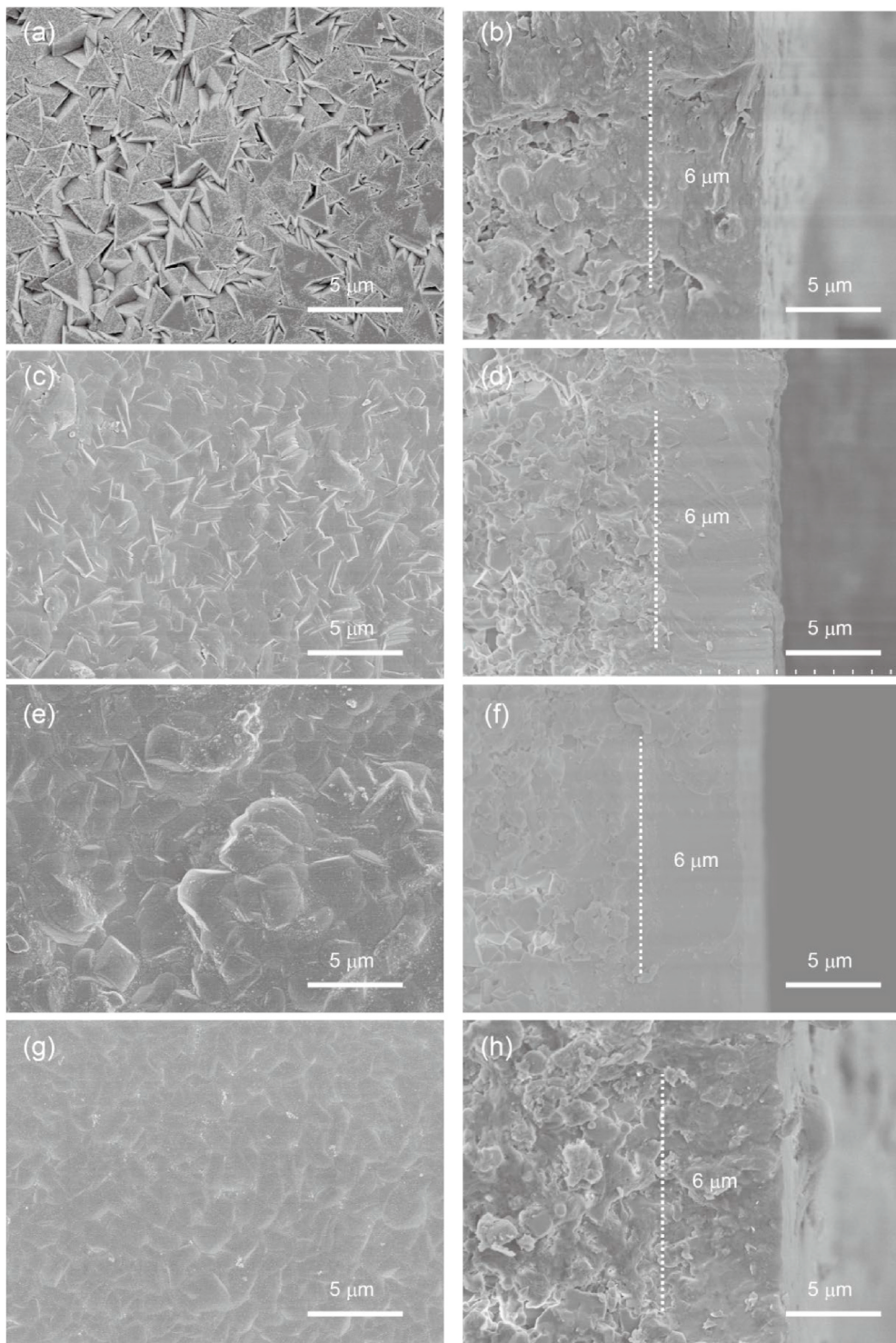


Fig. 1. Surface and cross-section SEM images of DD3R membranes. The $\text{SiO}_2/\text{Na}_2\text{O}$ ratio was 105 (a–b), 65 (c–d), 49 (e–f), 33 (g–h) and the synthesis was conducted at 140 °C for 44 h.

triangular crystals dominated the DD3R membrane surface at $\text{SiO}_2/\text{Na}_2\text{O}$ ratio of 105, wherein no extra NaOH added (Fig. 1a). This morphology was prevalent in the reported DD3R zeolite membranes [12,23], but the zeolite intergrowth seems insufficient in this work as evidenced by the gaps between crystals (Fig. 1a), which is probably due to industrial grade silica source adopted. As the $\text{SiO}_2/\text{Na}_2\text{O}$ ratio decreased to 65, the crystals fused together, and grain boundaries became blur (Fig. 1c). Meanwhile, the synthesis solution exhibited an increased pH value, which was up to 12.1 at the $\text{SiO}_2/\text{Na}_2\text{O}$ ratio of 33 (Table 2). The typical rhombic DD3R crystals preferred to form under a favorable pH value of 10–12 and the hexagonal prism were obtained from the synthesis solution with a pH value higher than 12.4 [19,20]. However, the content of structure directing agents (SDAs) can have an impact on the membrane morphology. It was noted that only irregular sphere was formed on the membrane synthesized at $\text{SiO}_2/\text{Na}_2\text{O}$ ratio of 33 in this work (Fig. 1g). Triangular crystals were even observed at the $\text{SiO}_2/\text{Na}_2\text{O}$ ratio of 6.7 in the case that the used SDAs was 5 times as high as ours [24].

To demonstrate the phase composition, the membranes synthesized with various alkalinity were characterized by PXRD (Fig. 2). The diffraction matched well with the simulated patterns from International Zeolite Association [25], proving a random orientation of the DDR crystals within the membranes. The XRD pattern of the DD3R membrane confirms the purity of the DDR crystalline phase, and no specified peaks of SGT and DOH phase were detected in these patterns. However, the peak intensity at $2\theta = 12.98^\circ$, 18.86° and 26.52° gradually diminished with the decrease of $\text{SiO}_2/\text{Na}_2\text{O}$ ratio from 105 to 33. The results indicating the zeolite crystallinity became worse. Similar phenomenon was observed on the powder collected from autoclave bottom and only amorphous substance was obtained in the case of $\text{SiO}_2/\text{Na}_2\text{O}$ ratio of 33. That would be the reason why a huge amount of SDAs were required at higher alkalinity in the literatures (such as $\text{SiO}_2/\text{Na}_2\text{O}$ ratio of 6.7) [24]. The membrane surface was further characterized by EDX analysis. The aluminum element was beyond the detection limitation of EDX technique, confirming the all-silica nature of our DDR zeolite membranes. While the aluminum was etched from the alumina support and incorporated into zeolite framework during the hydrothermal synthesis at high alkalinity [24]. In this case, cation ions usually present in the Al-containing zeolite for charge balance [26]; however, the element Na

Table 2

Synthesis solution property and the mixture separation performance of the corresponding membranes^a.

| No. | $\text{SiO}_2/\text{Na}_2\text{O}$ ^b | pH | Si/Al | P_{CO_2} ^c | \bar{P}_{CO_2} ^d | $\alpha_{\text{CO}_2/\text{CH}_4}$ | $\bar{\alpha}_{\text{CO}_2/\text{CH}_4}$ |
|-----|---|------|-----------|--------------------------------|--------------------------------------|------------------------------------|--|
| 1 | 105 ($x = 0.95$) | 11.1 | $+\infty$ | 14.1 | 11.4 ± 1.8 | 73 | 227 ± 85 |
| 2 | | | | 12.3 | 303 | | |
| 3 | | | | 8.1 | 300 | | |
| 4 | | | | 11.5 | 269 | | |
| 5 | | | | 10.8 | 153 | | |
| 6 | | | | 11.8 | 264 | | |
| 7 | 65 ($x = 1.54$) | 11.4 | $+\infty$ | 13.1 | 12.0 ± 0.9 | 326 | 466 ± 204 |
| 8 | | | | 12.2 | 211 | | |
| 9 | | | | 11.4 | 843 | | |
| 10 | | | | 10.4 | 576 | | |
| 11 | | | | 12.4 | 483 | | |
| 12 | | | | 12.6 | 356 | | |
| 13 | 49 ($x = 2.04$) | 11.8 | $+\infty$ | 9.1 | 9.2 ± 1.3 | 277 | 218 ± 43 |
| 14 | | | | 12.0 | 174 | | |
| 15 | | | | 9.2 | 204 | | |
| 16 | 33 ($x = 3.03$) | 12.1 | $+\infty$ | 7.9 | 10.6 ± 2.0 | 53 | 70 ± 40 |
| 17 | | | | 11.0 | 31 | | |
| 18 | | | | 13.0 | 126 | | |

^a Tested using 200 mL min⁻¹ equimolar mixture at 298 K and feed pressure of 0.2 MPa; swept with 100 mL min⁻¹ He at atmosphere pressure.

^b 100 SiO_2 : $x \text{Na}_2\text{O}$: 3 ADA: 50 EDA: 4000 H_2O .

^c Gas permeance, $\times 10^{-8}$ mol m⁻² s⁻¹ Pa⁻¹.

^d Averaged gas permeance, $\times 10^{-8}$ mol m⁻² s⁻¹ Pa⁻¹.

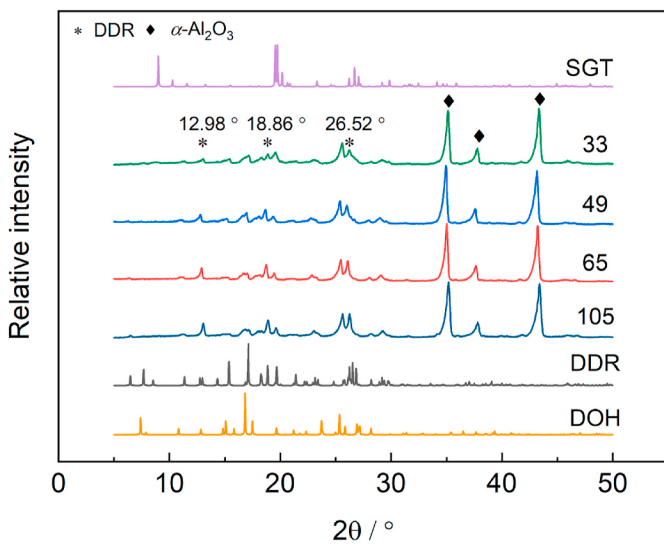


Fig. 2. XRD patterns of DD3R zeolite membranes synthesized with different $\text{SiO}_2/\text{Na}_2\text{O}$ ratio. Standard SGT, DDR, DOH zeolite patterns were shown for comparison [25].

was not detected either, further proving the neutral charge of the framework. This nature is highly desired in hydrogen separation to prevent the channel blockages by water vapor adsorption [27] and ethylene polymerization [28].

The membrane quality was initially evaluated by CO_2/CH_4 mixture separation prior to H_2 separation since DD3R zeolite membranes were intensively investigated for natural gas upgrading [13,29–31]. The test was conducted using equimolar CO_2/CH_4 mixture at room temperature and feed pressure of 0.2 MPa (Table 2). The membrane synthesized at $\text{SiO}_2/\text{Na}_2\text{O}$ ratio of 105 exhibited an averaged CO_2 permeance of $(1.14 \pm 1.8) \times 10^{-7}$ mol m⁻² s⁻¹ Pa⁻¹ and an averaged CO_2/CH_4 selectivity of (227 ± 85) . This was slightly lower than the membranes prepared from analytical reagent in our previous work [15,23]. However, the CO_2/CH_4 selectivity increased up to (466 ± 204) for $\text{SiO}_2/\text{Na}_2\text{O}$ ratio of 65, which is comparable to the results prepared from analytical reagent. The high separation performance of the membrane was in accordance with our SEM observations as mentioned above. The high selectivity is crucial to reduce the non-permeable components loss and energy consumption of the membrane separation [32]. With further decrease of the $\text{SiO}_2/\text{Na}_2\text{O}$ ratio, both the CO_2/CH_4 selectivity and CO_2 permeance declined. This is consistent with the decreased crystallinity of zeolite membrane, wherein the amorphous silica species were generated by crystal decomposition to block the zeolite pores [33]. Therefore, the synthesis solution with $\text{SiO}_2/\text{Na}_2\text{O}$ ratio of 65 was further used to scale-up synthesis of the membranes.

3.2. Scale-up synthesis of DD3R zeolite membranes

The optimized synthesis solution was further used to scale up the membranes with the length up to 25 cm. We designed a spacer allowing for the synthesis of 17 separate membranes in one autoclave, total 406 cm² effective area (Fig. 3a). The synthesis efficiency was improved twofold compared to the star-shaped spacer, which was previously used to 6 separate hollow fiber SAPO-34 zeolite membranes [34]. Both ends of the hollow fibers were sealed with PTFE tape and independently fixed on a spacer with outer diameter of 5 cm (Fig. 3b).

Total 51 pieces of DD3R zeolite membranes were obtained through three independent batch syntheses. Each membrane was evaluated by CO_2/CH_4 mixture separation at the same condition as mentioned above and shown in Table 3. Typically, Membrane 3-2 showed CO_2/CH_4 selectivity of 447 and CO_2 permeance of 1.55×10^{-7} mol m⁻² s⁻¹ Pa⁻¹. We also concerned the reproducibility in the scaled-up synthesis. As

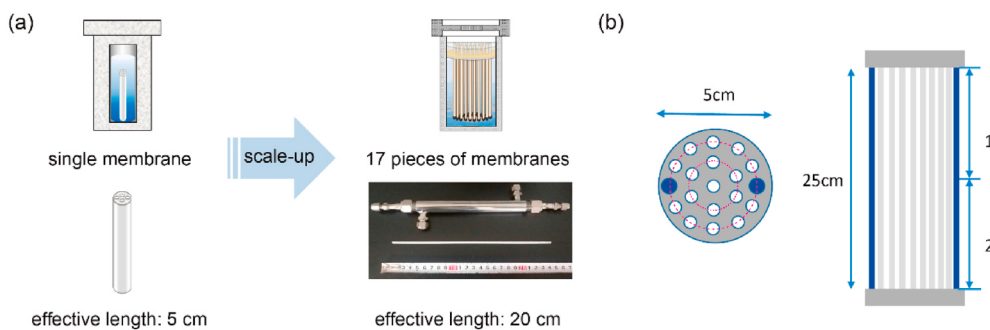


Fig. 3. Schematic diagram of the scale-up synthesis of DD3R zeolite membranes. (a) Batch-scale synthesis strategy, picture of 25 cm-length DD3R zeolite membrane and the corresponding module; (b) Position of the membranes in the autoclave.

Table 3

CO_2/CH_4 mixture separation performance of the batch-scale synthesized membranes^a.

| No. | P_{CO_2} ^b | $\alpha_{\text{CO}_2/\text{CH}_4}$ | No. | P_{CO_2} ^b | α | No. | P_{CO_2} ^b | $\alpha_{\text{CO}_2/\text{CH}_4}$ |
|------|--------------------------------|------------------------------------|------|--------------------------------|----------|------|--------------------------------|------------------------------------|
| 1-1 | 12.6 | 30 | 2-1 | 22.2 | 17 | 3-1 | 10.6 | 405 |
| 1-2 | 10.7 | 496 | 2-2 | 11.2 | 444 | 3-2 | 15.5 | 447 |
| 1-3 | 11.1 | 116 | 2-3 | 13.4 | 326 | 3-3 | 13.6 | 131 |
| 1-4 | 11.7 | 62 | 2-4 | 15.2 | 434 | 3-4 | 12.2 | 228 |
| 1-5 | 13.9 | 30 | 2-5 | 13.5 | 391 | 3-5 | 12.5 | 164 |
| 1-6 | 12.3 | 175 | 2-6 | 12.2 | 534 | 3-6 | 15.6 | 43 |
| 1-7 | 10.9 | 72 | 2-7 | 14.5 | 210 | 3-7 | 13.7 | 31 |
| 1-8 | 15.7 | 402 | 2-8 | 8.6 | 405 | 3-8 | 14.9 | 246 |
| 1-9 | 9.5 | 26 | 2-9 | 12.5 | 431 | 3-9 | 11.1 | 419 |
| 1-10 | 11.7 | 272 | 2-10 | 13.6 | 131 | 3-10 | 11.6 | 467 |
| 1-11 | 13.4 | 276 | 2-11 | 11.2 | 228 | 3-11 | 9.6 | 437 |
| 1-12 | 12.9 | 424 | 2-12 | 11.4 | 187 | 3-12 | 12.1 | 356 |
| 1-13 | 10.9 | 543 | 2-13 | 12.7 | 145 | 3-13 | 10.1 | 135 |
| 1-14 | 13.6 | 164 | 2-14 | 10.9 | 510 | 3-14 | 13.8 | 369 |
| 1-15 | 14.8 | 487 | 2-15 | 11.3 | 297 | 3-15 | 11.9 | 216 |
| 1-16 | 9.5 | 282 | 2-16 | 9.3 | 501 | 3-16 | 8.3 | 478 |
| 1-17 | 13.1 | 479 | 2-17 | 11.6 | 185 | 3-17 | 10.7 | 18 |

^a Tested using 200 mL min⁻¹ equimolar mixture at 298 K and feed pressure of 0.2 MPa; swept with 100 mL min⁻¹ He at atmosphere pressure.

^b Gas permeance, $\times 10^{-8}$ mol m⁻² s⁻¹ Pa⁻¹.

claimed by Baker and Low [32], the methane loss in membrane separation would be competitive to the amine absorption technology if the CO_2/CH_4 selectivity improved from 15 of the current cellulose acetate (CA) membrane to 25–30. In our scaled-up synthesis, only 3 pieces of membranes exhibited CO_2/CH_4 selectivity lower than 30. DD3R zeolite membranes are known for their outstanding selectivity. In the batch synthesis, about 82% of the synthesized membranes had the separation selectivity of higher than 100.

It has been well documented the synthesis gel would settle from the homogeneous synthetic solution to the bottom of the autoclaves [21, 35]. In this case, a thinner membrane layer formed on the top fragments because of the less nutrient concentration. To figure out if this affect on membrane crystallization, the membranes with selectivity less than 100 (Membrane 1–9, 2–1 and 3–11) were cut into two species, labelled as 1 and 2 from top to bottom as stood in the autoclave (Fig. 3b). The CO_2/CH_4 separation performance of each fragment was summarized in Table 4. The top fragment seems better than the bottom one in terms of selectivity for Membrane 1–9 and Membrane 2–1. However, the situation was reversed for Membrane 3–17. It means that the position had no contribution to poor selectivity. Since CO_2 permeance was inversely proportional to the thickness of defect-free DD3R zeolite membranes [36], the membranes with selectivity higher than 100 (Membrane 1–8, 1–15 and 1–17) were further evaluated as the poor-quality ones. No clear difference in CO_2 permeance between the top fragments and the bottom ones was observed either. However, a lower flux was demonstrated in the bottom fragments of T-type [35] and NaA zeolite [21]

Table 4

CO_2/CH_4 separation performance of DD3R-type zeolite membranes at different positions^a.

| No. | Position | P_{CO_2} ^b | $\alpha_{\text{CO}_2/\text{CH}_4}$ | No. | Position | P_{CO_2} ^b | $\alpha_{\text{CO}_2/\text{CH}_4}$ |
|-------------|----------|--------------------------------|------------------------------------|-------------|----------|--------------------------------|------------------------------------|
| 1–9 | 1 | 10.3 | 170 | 1–8 | 1 | 14.4 | 415 |
| | 2 | 9.3 | 4 | | 2 | 15.7 | 364 |
| 2–1 | 1 | 17.6 | 20 | 1–15 | 1 | 15.1 | 410 |
| | 2 | 21.5 | 12 | | 2 | 14.5 | 507 |
| 3–17 | 1 | 11.7 | 10 | 1–17 | 1 | 14.7 | 404 |
| | 2 | 9.1 | 30 | | 2 | 12.8 | 522 |

^a Tested using 200 mL min⁻¹ equimolar mixture at 298 K and feed pressure of 0.2 MPa; swept with 100 mL min⁻¹ He at atmosphere pressure.

^b Gas permeance, $\times 10^{-8}$ mol m⁻² s⁻¹ Pa⁻¹.

membranes for organic solvent dehydration. This can be explained by the dilute solution used in this work, wherein the nutrition sedimentation would be less compared to the gel precursors.

3.3. Single gas permeation

The single gas permeation of H_2 , CO_2 , N_2 , CH_4 and SF_6 was conducted to evaluate the scaled-up membrane quality. As shown in Fig. 4a, the CO_2 permeance of 25 cm long DD3R zeolite membrane was maximized and the other single gas permeance followed the order of $\text{H}_2 > \text{N}_2 > \text{CH}_4 \gg \text{SF}_6$. Because of the much larger kinetic diameter of SF_6 (0.51 nm) than the pore size of DDR (0.36 × 0.44 nm), the non-zeolitic pores are deemed as the exclusive pathway for SF_6 permeation [23]. The pure component SF_6 permeance was determined to be 5.1×10^{-12} mol m⁻² s⁻¹ Pa⁻¹ at feed pressure of 0.4 MPa, which was three magnitude lower than the H_2 permeance. The ideal H_2/SF_6 selectivity was up to 2000 confirming the defect-free nature of the scaled-up DD3R zeolite membranes.

Considering the presence of C_2H_4 and C_2H_6 in the cracked gas stream, their single gas permeation was also tested (Fig. 4b). The single component permeance of H_2 exhibited a value of 1.8×10^{-8} mol m⁻² s⁻¹ Pa⁻¹ at 303 K and feed pressure of 0.4 MPa. With temperature increased up to 373 K the activated H_2 diffusion was not expected [36, 37]. The apparent activation energy gave a value of $-2.13 \text{ kJ mol}^{-1}$, which matched well with the results from Kapteijn et al. (-2.9 kJ mol^{-1}) [38]. This is reasonable because the H_2 diffusion through DDR pores is like Knudsen permeation below 373 K [37, 38]. The single component permeance at 303 K decreased to 1.4×10^{-10} mol m⁻² s⁻¹ Pa⁻¹ for CH_4 , 0.72×10^{-10} mol m⁻² s⁻¹ Pa⁻¹ for C_2H_4 and 0.41×10^{-10} mol m⁻² s⁻¹ Pa⁻¹ for C_2H_6 , respectively, mainly due to the strong size-exclusion effects. The ideal selectivity of H_2 over CH_4 , C_2H_4 and C_2H_6 was 124, 242 and 424, which is much higher than the Knudsen selectivity (Fig. 4c). The H_2/CH_4 ideal selectivity decreased with temperature while the situation was reversed for $\text{H}_2/\text{C}_2\text{H}_4$ and $\text{H}_2/\text{C}_2\text{H}_6$.

To explain the above phenomenon, single-component isotherms of H_2 , CH_4 , C_2H_4 and C_2H_6 were collected at 298 K (Fig. 5). Even the kinetic

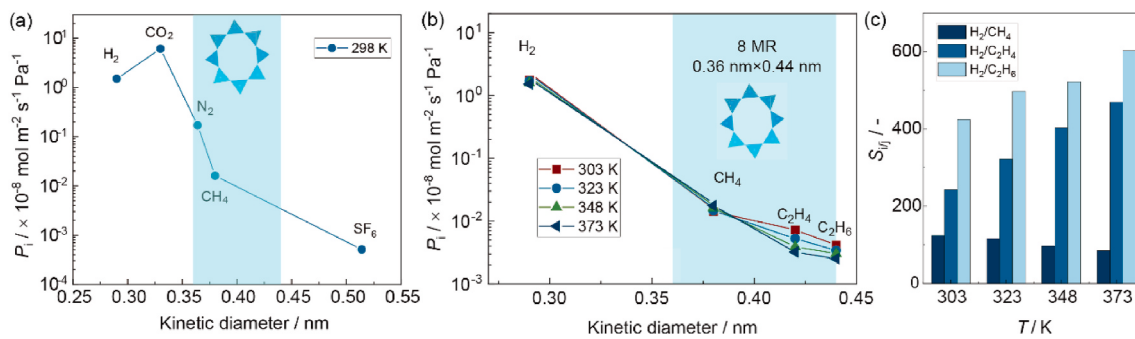


Fig. 4. Dependence of single gas permeance on kinetic diameters. (a) 25 cm long Membrane 1–13; (b) 5 cm long Membrane 1-17-2; (c) ideal selectivity of H_2 over CH_4 , C_2H_4 and C_2H_6 . The test was conducted at 0.4 MPa feed pressure, atmospheric pressure on permeate side and no sweep gas used.).

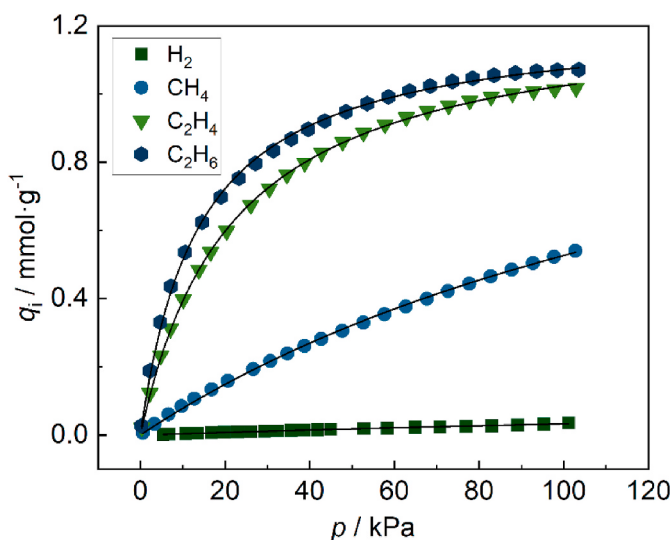


Fig. 5. Single component adsorption isotherms of H_2 , CH_4 , C_2H_4 and C_2H_6 at 298 K.

diameter of C_2H_6 (0.44 nm) is larger than the aperture size of DDR zeolite, the adsorption was higher than the other components and the adsorption amount followed the order of $\text{C}_2\text{H}_6 > \text{C}_2\text{H}_4 > \text{CH}_4 \gg \text{H}_2$. The IAST (Ideal Adsorbed Solution Theory) adsorption selectivity was 20 for CH_4/H_2 , 100 for $\text{C}_2\text{H}_4/\text{H}_2$, 104 for $\text{C}_2\text{H}_6/\text{H}_2$ in the equimolar binary mixture at 100 kPa. The preferential adsorption of hydrocarbons is unfavorable to H_2 permeation because of the single-file diffusion behavior in zeolitic channels [28]. The diffusivity is facilitated at the elevated temperature while the slow components (CH_4 , C_2H_4 , C_2H_6) would benefit more. This is the reason why the CH_4 permeance increased with temperature [29,31], which should be applied to other slow components. However, the permeance of C_2H_4 and C_2H_6 decreased with temperature increasing from 303 K to 373 K (Fig. 4b). The single component adsorption of C_2H_4 and C_2H_6 is more sensitive to temperature because of the stronger interaction with DD3R zeolite (Table 5). Since the gas permeation is well explained by the surface diffusion mechanism [36, 38], we believe the uptake reduction exceeded the increase of diffusivity in the case of C_2H_4 and C_2H_6 .

Table 5
Gas adsorption parameters on DD3R zeolite at 298 K.

| Gas | $q^{\text{sat}} / \text{mol kg}^{-1}$ | $K / \times 10^{-3} \text{ kPa}^{-1}$ | $-\Delta H_{\text{ads}} / \text{kJ mol}^{-1}$ | Ref |
|------------------------|---------------------------------------|---------------------------------------|---|------|
| H_2 | 3.66 | 0.08 | 5.6 | [38] |
| CH_4 | 1.89 | 3.27 | 17.3 | [36] |
| C_2H_4 | 1.27 | 31.92 | 24.29 | [39] |
| C_2H_6 | 1.31 | 34.30 | 24.76 | |

3.4. Mixed gas separation

To achieve more insights, the binary mixtures were further used to evaluate the H_2 permeation. In the case of H_2/CH_4 mixture, H_2 permeance matched well with the one of single component (<0.6% fluctuation) and gradually decreased with temperature from $2.4 \times 10^{-8} \text{ mol m}^{-2} \text{ s}^{-1} \text{ Pa}^{-1}$ (330 barrer) at 298 K to $1.5 \times 10^{-8} \text{ mol m}^{-2} \text{ s}^{-1} \text{ Pa}^{-1}$ at 373 K (Fig. 6a), which is thirty times higher than that of commercial polymeric membranes [5]. While the CH_4 permeance slightly increased causing a decreasing H_2/CH_4 selectivity from 177 at 298 K to 109 at 373 K. However, a reverse situation was observed in the $\text{H}_2/\text{C}_2\text{H}_4$ mixture (Fig. 6b). The H_2 permeance was 21% of single component at 243 K and increased simultaneously with the decrease of C_2H_4 permeance until approaching the maximum at 373 K. The H_2 permeance was $1.4 \times 10^{-8} \text{ mol m}^{-2} \text{ s}^{-1} \text{ Pa}^{-1}$ at 323 K, which was 70% of the H_2 permeance in H_2/CH_4 mixture separation. The result indicates H_2 permeation is more hindered by the component of C_2H_4 than that of CH_4 . The situation was even worse (Fig. 6c) in $\text{H}_2/\text{C}_2\text{H}_6$ because of the stronger interaction with DD3R zeolite as proven by the single component adsorption (Table 5). This could be well evidenced by the even lower H_2 permeance, which was merely 39% of the single component permeance at 323 K. Meanwhile the $\text{H}_2/\text{C}_2\text{H}_6$ selectivity was more sensitive to temperature and increased to 166 at 323 K.

The binary mixture separation was also conducted under various pressure (Fig. 6d–f). All the H_2 permeance decreased because of the enhanced competitive adsorption of hydrocarbons with H_2 at elevated pressure [36]. However, the H_2/CH_4 selectivity was still as high as 107 together with a H_2 permeance of $1.71 \times 10^{-8} \text{ mol m}^{-2} \text{ s}^{-1} \text{ Pa}^{-1}$ at the feed pressure of 0.5 MPa (Fig. 6d). The CH_4 permeance increased with pressure as observed from previous literatures [15,30]. The molecular dynamic simulation revealed that the diffusivity of CH_4 increased with loading because of the reduced adsorbate-adsorbate interactions [31]. The permeance of C_2H_4 and C_2H_6 remains constant with pressure, indicating the permeation flux was linearly related to the feed pressure. Considering the Langmuir type isotherms of C_2H_4 and C_2H_6 , the driving force for the permeation actually was non-linear. Therefore, we speculated the diffusivity increased more with pressure, compensating for the less increased driving force. Previously Ruthven et al. [40] reported an increased diffusivity with loading even the pressure (210 mbar) was far less here. While the H_2 permeance decreased to $0.39 \times 10^{-8} \text{ mol m}^{-2} \text{ s}^{-1} \text{ Pa}^{-1}$ with a selectivity of 54 in the $\text{H}_2/\text{C}_2\text{H}_6$ mixture at feed pressure of 0.5 MPa. This is well explained by the increased hydrocarbon uptake at elevated pressure and the blockage to H_2 molecule enter/diffuse through the zeolitic channels [38].

To quantify the channel blockage effect, C_2H_4 or C_2H_6 was gradually added into the equimolar H_2/CH_4 mixture. Because H_2 permeation is like Knudsen diffusion [37,41], the permeance should be independent on the partial pressure. Therefore, the uptake of C_2H_4 or C_2H_6 would be the key factor to determine the H_2 permeance. As indicated by the single component adsorption isotherms (Fig. 5), the uptake of C_2H_4 and C_2H_6

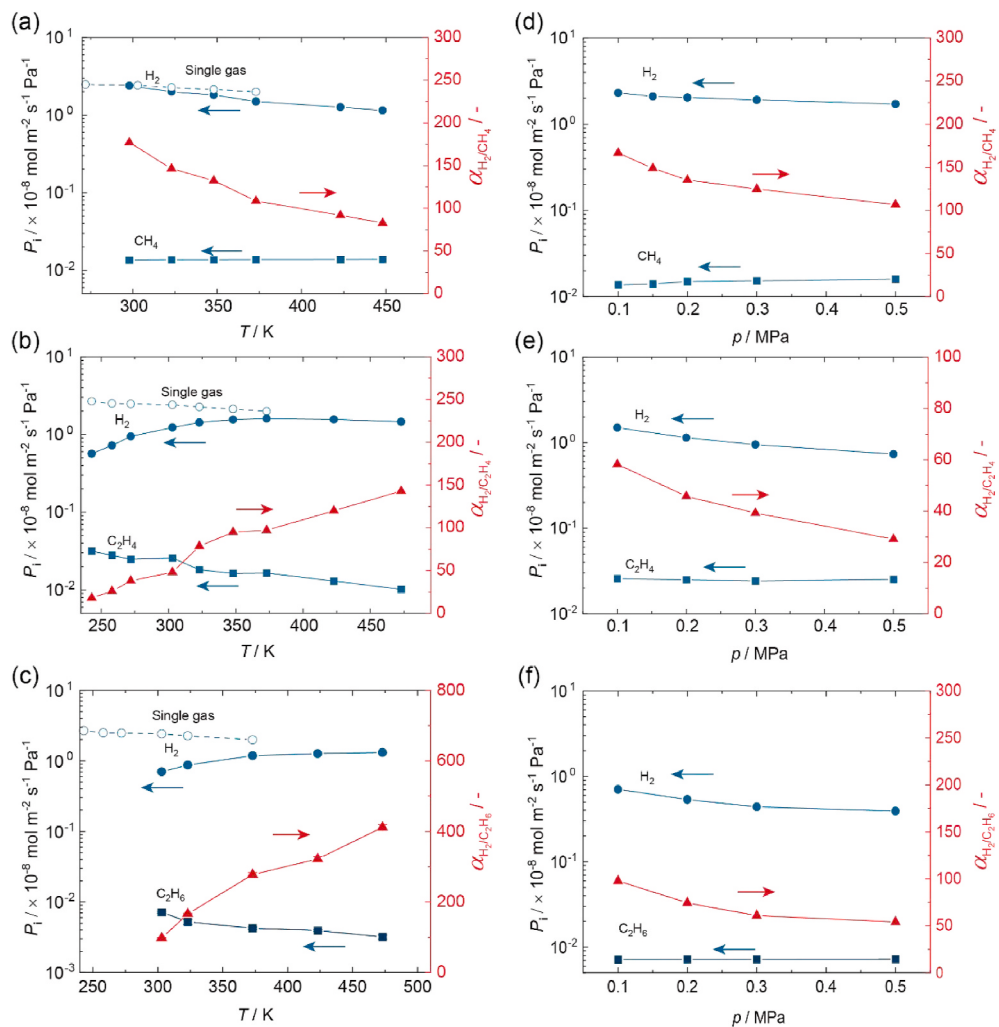


Fig. 6. Single component H₂ permeation and mixed gas separation performance for H₂/CH₄, H₂/C₂H₄ and H₂/C₂H₆. (a–c) Temperature-dependent performance at feed pressure of 0.1 MPa, (d–f) Pressure-dependent performance at room temperature. Membrane 1-17-2 was used for the test using He as the sweep gas. Closed symbols: equimolar gas mixture; Open symbols: Single component H₂.

rapidly increased initially with pressure. The H₂ permeance was 2.2 × 10⁻⁸ mol m⁻² s⁻¹ Pa⁻¹ and monotonically decreased with the increasing partial pressure of C₂H₄ and C₂H₆ (Fig. 7). The H₂ permeance decreased by 23% once the C₂H₄ partial pressure increased to 13 kPa. In the case of C₂H₆, the reduction was up to 37% because of the stronger interaction. To visualize the effects of channel blockage on H₂ permeation, the relative reduction of H₂ permeance ($\Delta P_{H_2}'$) was calculated and plotted together with the C₂H₄/C₂H₆ uptake (Fig. 8). The $\Delta P_{H_2}'$ followed the trend of C₂ uptake with increasing partial pressure which also can be

expressed in a linear relationship. Therefore, the decrease of H₂ permeance was due to the competitive adsorption of C₂H₄ or C₂H₆ on the zeolite pores.

3.5. Membrane stability

To demonstrate the feasibility of practical application, DD3R zeolite membrane was used to separate H₂ from the simulated cracked gas of ethylene plants. Because the heavy hydrocarbons (>C₃) can be

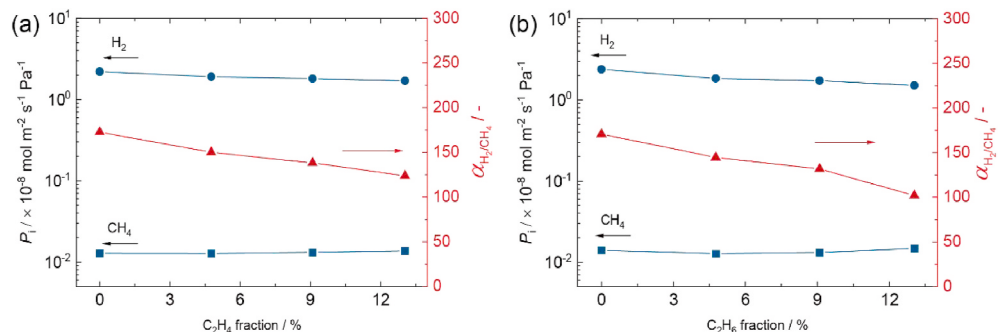


Fig. 7. Effect of the molar fraction of ethylene (a) and ethane (b) on the equimolar H₂/CH₄ mixture separation at room temperature and feed pressure of 0.1 MPa. Membrane 1-17-2 was used for the test using He as the sweep gas.

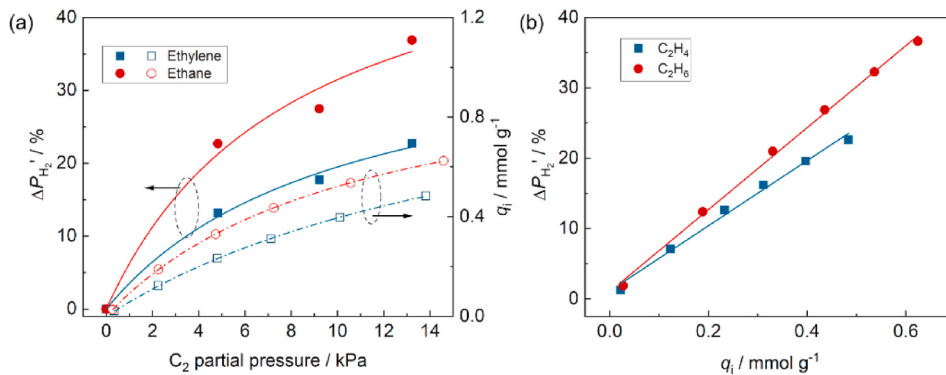


Fig. 8. The relative reduction of H₂ permeance ($\Delta P_{H_2}'$) with the increase of the partial pressure (a) C₂H₄/C₂H₆ uptake (b). Test condition: equimolar H₂/CH₄ mixture at room temperature and feed pressure of 0.1 MPa. Solid line was guided for observation.

efficiently removed in the pre-depropanization separation process, only the impurity of C₁ and C₂ species was present in the feed with a composition of 20 H₂: 30 CH₄: 45 C₂H₄: 5 C₂H₆. The temperature-dependent H₂ separation performance was collected at atmosphere pressure (Fig. 9). The H₂ permeance at 298 K was $0.86 \times 10^{-8} \text{ mol m}^{-2} \text{s}^{-1} \text{ Pa}^{-1}$ which is lower than the single H₂ permeance but approaching the one in H₂/C₂H₄ binary mixture (shown in Fig. 6b). The C₂H₄ permeance decreased with temperature because of the less uptake, leading to a mitigated blocking effect to H₂ permeation. The H₂/C₂H₄ selectivity significantly increased with temperature while the one of H₂/CH₄ seemed to level-off at 353 K. We argued the H₂ permeation was more sensitive to the presence of strong interaction components (C₂H₄ or C₂H₆). Therefore, it is preferred to separate H₂ at elevated temperature from cracked gas in the view point of maximizing membrane performance.

Besides the membrane performance, the stability is another critical criterion to the practical application. We have demonstrated DD3R zeolite membranes were stable in wet gas atmosphere for more than 300 h [15,23]. Thus the resistance to high pressure feed (Fig. 10) and H₂S poisoning (Fig. 11) was more concerned here. A consistent H₂ permeance was achieved, indicating the hydrogen flux (throughput) would be easily improved by increasing the feed pressure. The CH₄ permeance gradually increased with pressure, which is explained by the increased uptake and improved diffusivity [31]. However, the H₂/CH₄ selectivity was still up to 50 at 2.1 MPa. Similar selectivity of 56 was achieved when the permeate was ventilated by vacuum pump. The beneficial throughput and selectivity guarantee DD3R zeolite membranes a reliable hydrogen separation from the realistic cracked gas under high

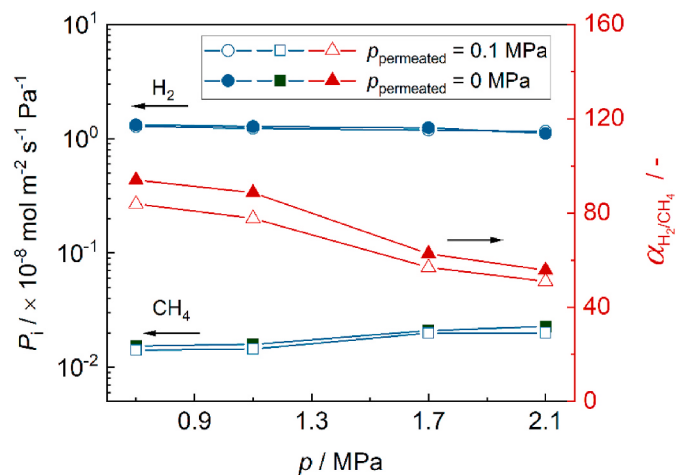


Fig. 10. High-pressure separation performance of 25 cm long DD3R zeolite membrane. The feed was equimolar H₂/CH₄ mixture at room temperature and the permeate was kept at vacuum or atmosphere pressure without sweep gas. Membrane 1–13 was used for the test.

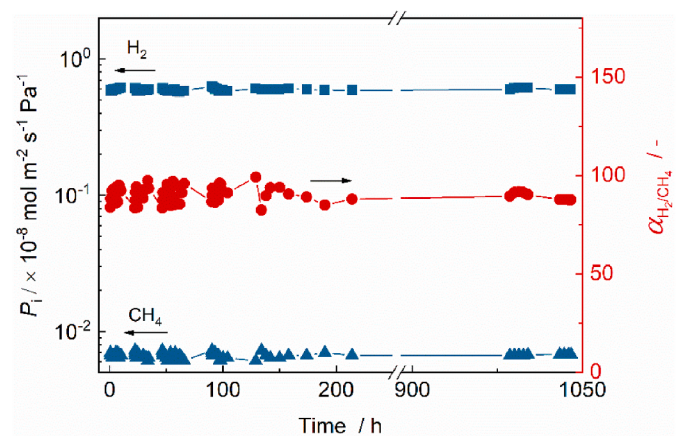


Fig. 11. Long-term stability of zeolite membranes in 100 ppm H₂S-containing feed at 303 K and 0.2 MPa. Feed composition: 20H₂: 30 CH₄: 45 C₂H₄: 5 C₂H₆, flow rate: 100 mL min⁻¹. Membrane 1–13 was used for the test.

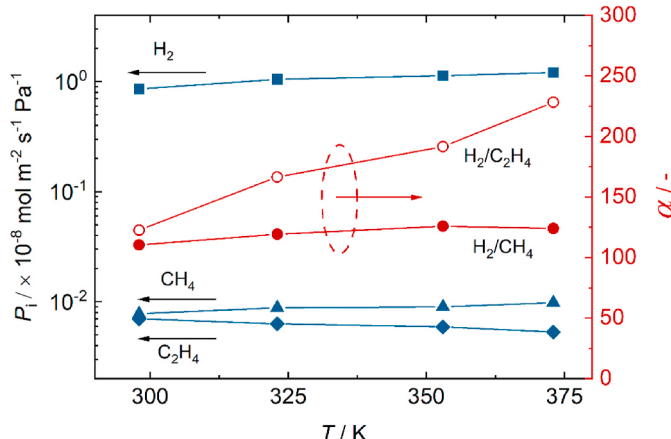


Fig. 9. Separation performance of DD3R zeolite membrane in simulated cracked gas of ethylene plants. Feed composition was 20H₂: 30 CH₄: 45 C₂H₄: 5 C₂H₆ and pressure was 0.1 MPa. Membrane 1-17-2 was used for the test.

pressure. Even H₂ and CH₄ are no plasticizing gas, the C₂₊ hydrocarbons existed in the actual system still has proved to be particularly troublesome for polymeric membrane because of the plasticization phenomenon [42]. The plasticization pressure of ethylene and ethane was ~ 1

MPa for polyimide and the mole fraction of ethylene in the simulated gas of the ethylene plant is as high as ~45%, which limits the application of polymeric membranes in the ethylene plant [43].

The DD3R zeolite membrane was stable in H₂S-containing gas for more than 1000 h as shown in Fig. 11. Initially, the on-stream test was conducted in simulated cracked gas containing 100 ppm H₂S. Because of the presence of ethane and ethylene, the H₂ permeance was relatively low at 0.6×10^{-8} mol m⁻² s⁻¹ Pa⁻¹ and the H₂/CH₄ selectivity was about 90 over the 200 h operation. Then the membrane was left in the feed atmosphere and the data collection was interrupted. After 800 h exposure to H₂S, the membrane performance was tracked again. Both the permeance and selectivity were consistent with the initial performance. However, the Pd membrane, an ultrahigh H₂-selective membrane, would be poisoned by 5 ppm H₂S to form a dense sulphide layer, which leads a reduced H₂ permeance [44].

4. Conclusions

The industrial grade silica gel was applied to scale-up the hollow fiber DD3R zeolite membranes. To improve the membrane quality, it was crucial to control the alkalinity of synthesis solution. The optimized SiO₂/Na₂O ratio was determined to be 65 regardless of the silica source. We designed a spacer to synthesize 17 separate membranes with 406 cm² in one batch and about 82% of the synthesized membranes had the separation selectivity of higher than 100. Typically, the 25 cm long membrane showed CO₂/CH₄ selectivity of 447 and CO₂ permeance of 1.55×10^{-7} mol m⁻² s⁻¹ Pa⁻¹. The single component permeance of H₂ exhibited a value of 1.8×10^{-8} mol m⁻² s⁻¹ Pa⁻¹ at 303 K and 0.4 MPa feed pressure, leading to the ideal selectivity of 124 for H₂/CH₄, 242 for H₂/C₂H₄ and 424 for H₂/C₂H₆ at 303 K. The permeance decreased by 48.7% and 70.9% once the feed was switched from single component H₂ to equimolar binary mixture with C₂H₄ and C₂H₆ at 303 K, respectively. The surface barrier derived from strong interaction components (such as ethylene and ethane) hindered the H₂ molecules entering the zeolite pores and diffusing through the membrane. The blocking effect was enhanced with pressure because of the enhanced competitive adsorption. However, the H₂ permeation in multi-components was approaching the trend of binary mixture containing the strong interaction component. The DD3R zeolite membrane was stable for more than 1000 h in the simulated cracked gas containing 100 ppm H₂S. Together with the linear increase of H₂ flux and H₂/CH₄ separation selectivity of 50 at high pressure of 2.1 MPa, DD3R zeolite membranes pave the way to H₂ separation from ethylene industry.

Author statement

Peng Du: Conceptualization, Methodology, Data curatio, Visualization, Writing-Original Draft. **Jieyu Song:** Methodology, Data curation, Investigation. **Xuerui Wang:** Validation, Writing-Reviewing and Editing, Funding acquisition. **Yuting Zhang:** Resources, Investigation. **Jixian Xie:** Methodology, Investigation. **Gang Liu:** Investigation. **Yongli Liu:** Investigation. **Zhenwei Wang:** Investigation. **Zhou Hong:** Resources. **Xuehong Gu:** Supervision, Project administration, Writing-Reviewing and Editing, Funding acquisition.

Declaration of competing interest

The authors declare that they have no known competing financial interests or personal relationships that could have appeared to influence the work reported in this paper.

Acknowledgement

This work is sponsored by National Natural Science Foundation of China (22035002, 21908097 and 21808106), the Leading Talent in Ten-Thousand Talent Program (2019), Jiangsu Specially-Appointed

Professors Program (2019) and State Key Laboratory of Materials-Oriented Chemical Engineering (ZK202002).

References

- [1] P. Bernardo, A. Criscuoli, G. Clarizia, G. Barbieri, E. Drioli, G. Fleres, M. Picciotti, Applications of membrane unit operations in ethylene process, *Clean Technol. Environ. Policy* 6 (2004) 78–95.
- [2] A.A. Garcia Blanco, A.F. Vallone, A. Gil, K. Sapag, A comparative study of various microporous materials to store hydrogen by physical adsorption, *Int. J. Hydrogen Energy* 37 (2012) 14870–14880.
- [3] M. Carta, R. Malpass-Evans, M. Croad, Y. Rogan, J.C. Jansen, P. Bernardo, F. Bazzarelli, N.B. McKeown, An efficient polymer molecular sieve for membrane gas separations, *Science* 339 (2013) 303–307.
- [4] A. Mivechian, M. Pakizeh, Hydrogen recovery from Tehran refinery off-gas using pressure swing adsorption, gas absorption and membrane separation technologies: simulation and economic evaluation, *J. Chem. Eng. Chin. Univ.* 30 (2013) 937–948.
- [5] M. Yáñez, A. Ortiz, D. Gorri, I. Ortiz, Comparative performance of commercial polymeric membranes in the recovery of industrial hydrogen waste gas streams, *Int. J. Hydrogen Energy* 46 (2021) 17507–17521.
- [6] X. Wang, C. Chi, K. Zhang, Y. Qian, K.M. Gupta, Z. Kang, J. Jiang, D. Zhao, Reversed thermo-switchable molecular sieving membranes composed of two-dimensional metal-organic nanosheets for gas separation, *Nat. Commun.* 8 (2017) 14460.
- [7] J. Jiang, S. Islam, Q. Dong, F. Zhou, S. Li, M. Yu, Deposition of an ultrathin palladium (Pd) coating on SAPO-34 membranes for enhanced H₂/N₂ separation, *Int. J. Hydrogen Energy* 45 (2020) 33648–33656.
- [8] X. Gao, C. Da, C. Chen, Z. Li, X. Gu, S.K. Bhatia, The induced orientation effect of linear gases during transport in a NaA zeolite membrane modified by alkali lignin, *J. Membr. Sci.* (2021), <https://doi.org/10.1016/j.memsci.2020.118971>.
- [9] X. Gu, Z. Tang, J. Dong, On-stream modification of MFI zeolite membranes for enhancing hydrogen separation at high temperature, *Microporous Mesoporous Mater.* 111 (2008) 441–448.
- [10] J.C. Poschuta, V.A. Tuan, E.A. Pape, R.D. Noble, J.L. Falconer, Separation of light gas mixtures using SAPO-34 membranes, *AIChE J.* 46 (2000) 779–789.
- [11] J. van den Bergh, C. Güçüyener, J. Gascon, F. Kapteijn, Isobutane dehydrogenation in a DD3R zeolite membrane reactor, *Chem. Eng. J.* 166 (2011) 368–377.
- [12] T. Tomita, K. Nakayama, H. Sakai, Gas separation characteristics of DDR type zeolite membrane, *Microporous Mesoporous Mater.* 68 (2004) 71–75.
- [13] J. Okazaki, H. Hasegawa, N. Chikamatsu, K. Yajima, K. Shimizu, M. Niino, DDR-type zeolite membrane: a novel CO₂ separation technology for enhanced oil recovery, *Separ. Purif. Technol.* 218 (2019) 200–205.
- [14] M. Muhammad, Y.F. Yeong, K.K. Lau, A.B.M. Shariff, Issues and challenges in the development of Deca-Dodecasil 3 Rhombohedral membrane in CO₂ capture from natural Gas, *Separ. Purif. Rev.* 44 (2015) 331–340.
- [15] L. Wang, C. Zhang, X. Gao, L. Peng, J. Jiang, X. Gu, Preparation of defect-free DDR zeolite membranes by eliminating template with ozone at low temperature, *J. Membr. Sci.* 539 (2017) 152–160.
- [16] Y. Zhang, S. Chen, R. Shi, P. Du, X. Qiu, X. Gu, Pervaporation dehydration of acetic acid through hollow fiber supported DD3R zeolite membrane, *Separ. Purif. Technol.* 204 (2018) 234–242.
- [17] N. Kosinov, C. Auffret, C. Gucuyener, B.M. Szyja, J. Gascon, F. Kapteijn, E.J. M. Hensen, High flux high-silica SSZ-13 membrane for CO₂ separation, *J. Mater. Chem. A* 2 (2014) 13083–13092.
- [18] J. Gascon, W. Blom, A. van Miltenburg, A. Ferreira, R. Berger, F. Kapteijn, Accelerated synthesis of all-silica DD3R and its performance in the separation of propylene/propane mixtures, *Microporous Mesoporous Mater.* 115 (2008) 585–593.
- [19] S. Yang, J. Provenzano, A. Arvanitis, W. Jing, J. Dong, Morphological control of DDR zeolite crystals in Sigma-1 assisted hydrothermal synthesis using reduced organic agents, *J. Porous Mater.* 21 (2014) 1001–1007.
- [20] M. Wang, M. Li, M. Wang, Y. Zhang, L. Bai, Y. Zhang, Fine control of crystal morphologies of all-silica DDR in ethylenediamine-free gel with inorganic base as mineralizing agent, *Microporous Mesoporous Mater.* 288 (2019) 109596.
- [21] Y. Liu, X. Wang, Y. Zhang, Y. He, X. Gu, Scale-up of NaA zeolite membranes on α -Al₂O₃ hollow fibers by a secondary growth method with vacuum seeding, *Chin. J. Chem. Eng.* 23 (2015) 1114–1122.
- [22] H. Liu, X. Gao, S. Wang, Z. Hong, X. Wang, X. Gu, SSZ-13 zeolite membranes on four-channel α -Al₂O₃ hollow fibers for CO₂ separation, *Separ. Purif. Technol.* (2021), <https://doi.org/10.1016/j.seppur.2021.118611>.
- [23] X. Wang, Y. Zhang, X. Wang, E. Andres-Garcia, P. Du, L. Giordano, L. Wang, Z. Hong, X. Gu, S. Murad, F. Kapteijn, Xenon recovery by DD3R zeolite membranes: application in Anaesthetics, *Angew. Chem. Int. Ed.* 58 (2019) 15518–15525.
- [24] M. Wang, L. Bai, M. Li, L. Gao, M. Wang, P. Rao, Y. Zhang, Ultrafast synthesis of thin all-silica DDR zeolite membranes by microwave heating, *J. Membr. Sci.* 572 (2019) 567–579.
- [25] International Zeolite Association, accessed, <https://america.iza-structure.org/IZA-SC/framework.php?STC=DDR>, 2021. (Accessed 17 March 2021).
- [26] S. Li, J. Li, M. Dong, S. Fan, T. Zhao, J. Wang, W. Fan, Strategies to control zeolite particle morphology, *Chem. Soc. Rev.* 48 (2019) 885–907.
- [27] X. Wang, T. Zhou, P. Zhang, W. Yan, Y. Li, L. Peng, D. Veerman, M. Shi, X. Gu, F. Kapteijn, High-silica CHA zeolite membrane with ultra-high selectivity and irradiation stability for Krypton/Xenon separation, *Angew. Chem. Int. Ed.* 133 (2021) 9114–9119.

- [28] X. Wang, Y. Chen, C. Zhang, X. Gu, N. Xu, Preparation and characterization of high-flux T-type zeolite membranes supported on YSZ hollow fibers, *J. Membr. Sci.* 455 (2014) 294–304.
- [29] J. van den Bergh, W. Zhu, J.C. Groen, F. Kapteijn, J.A. Moulijn, K. Yajima, K. Nakayama, T. Tomita, S. Yoshida, Natural gas purification with a DDR zeolite membrane; permeation modelling with maxwell-stefan equations, in: R. Xu, Z. Gao, J. Chen, W. Yan (Eds.), *Stud. Surf. Sci. Catal.*, Elsevier, 2007, pp. 1021–1027.
- [30] S. Himeno, T. Tomita, K. Suzuki, K. Nakayama, K. Yajima, S. Yoshida, Synthesis and permeation properties of a DDR-type zeolite membrane for separation of CO₂/CH₄ gaseous mixtures, *Ind. Eng. Chem. Res.* 46 (2007) 6989–6997.
- [31] S.E. Jee, D.S. Sholl, Carbon dioxide and methane transport in DDR zeolite: insights from molecular simulations into carbon dioxide separations in small pore zeolites, *J. Am. Chem. Soc.* 131 (2009) 7896–7904.
- [32] R.W. Baker, B.T. Low, Gas separation membrane materials: a perspective, *Macromolecules* 47 (2014) 6999–7013.
- [33] Z. Wu, C. Zhang, L. Peng, X. Wang, Q. Kong, X. Gu, Enhanced stability of MFI zeolite membranes for separation of ethanol/water by eliminating surface Si-OH groups, *ACS Appl. Mater. Interfaces* 10 (2018) 3175–3180.
- [34] P.S. Lee, M.S. Lim, A. Park, H. Park, S.-E. Nam, Y.-I. Park, A zeolite membrane module composed of SAPO-34 hollow fibers for use in fluorinated gas enrichment, *J. Membr. Sci.* 542 (2017) 123–132.
- [35] M. Ji, X. Gao, X. Wang, Y. Zhang, J. Jiang, X. Gu, An ensemble synthesis strategy for fabrication of hollow fiber T-type zeolite membrane modules, *J. Membr. Sci.* 563 (2018) 460–469.
- [36] J. van den Bergh, W. Zhu, J. Gascon, J.A. Moulijn, F. Kapteijn, Separation and permeation characteristics of a DD3R zeolite membrane, *J. Membr. Sci.* 316 (2008) 35–45.
- [37] M. Kanezashi, J. O'Brien-Abraham, Y.S. Lin, K. Suzuki, Gas permeation through DDR-type zeolite membranes at high temperatures, *AIChE J.* 54 (2008) 1478–1486.
- [38] J. van den Bergh, A. Tihaya, F. Kapteijn, High temperature permeation and separation characteristics of an all-silica DDR zeolite membrane, *Microporous Mesoporous Mater.* 132 (2010) 137–147.
- [39] W. Zhu, F. Kapteijn, J.A. Moulijn, M.C. Den Exter, J.C. Jansen, Shape selectivity in adsorption on the all-silica DD3R, *Langmuir* 16 (2000) 3322–3329.
- [40] T. Binder, C. Chmelik, J. Kärger, A. Martinez-Joaristi, J. Gascon, F. Kapteijn, D. Ruthven, A diffusion study of small hydrocarbons in DDR zeolites by micro-imaging, *Microporous Mesoporous Mater.* 180 (2013) 219–228.
- [41] P.F. Zito, A. Caravella, A. Brunetti, E. Drioli, G. Barbieri, CO₂/H₂ selectivity prediction of NaY, DD3R, and silicalite zeolite membranes, *Ind. Eng. Chem. Res.* 57 (2018) 11431–11438.
- [42] M. Galizia, W.S. Chi, Z.P. Smith, T.C. Merkel, R.W. Baker, B.D. Freeman, 50th anniversary perspective: polymers and mixed matrix membranes for gas and vapor separation: a review and prospective opportunities, *Macromolecules* 50 (2017) 7809–7843.
- [43] J.E. Bachman, Z.P. Smith, T. Li, T. Xu, J.R. Long, Enhanced ethylene separation and plasticization resistance in polymer membranes incorporating metal-organic framework nanocrystals, *Nat. Mater.* 15 (2016) 845–849.
- [44] T.A. Peters, M. Stange, P. Veenstra, A. Nijmeijer, R. Bredesen, The performance of Pd–Ag alloy membrane films under exposure to trace amounts of H₂S, *J. Membr. Sci.* 499 (2016) 105–115.